Front. Chem. China (2006) 2: 161–169
DOI 10.1007/s 11458-006-0021-1

RESEARCH ARTICLE

Wang Tingting, Zeng Heping

Synthesis, charge-separated state characterization of *N*-methyl-2-(4'-*N*-ethylcarbozole)-3-fulleropyrrolidine and its derivatives

Abstract *N*-Methyl-2-(*N*-ethylcarbozole)- fulleropyrro lidine and *N*-methyl-2- (4'-*N*,*N*- diphenylaminophenyl)- fulleropyrrolidine were synthesized by 1,3-dipolar cycloaddition under microwave irradiation, which were characterized by MS, ^{1}H NMR, IR and UV–Vis. Photoinduced intramolecular electron transfer process from C_{60} moiety to carbazole moiety has been studied by nanosecond laser flash photolysis. The charge-separated state $C_{60}^{\bullet-}$–$Cz^{\bullet+}$ was observed in the near-IR region with a lifetime of 0.28 μs. The electronic spectrum of the C_{60}-TPA was studied by using ZINDO method on the basis of the optimized geometrics with B3LYP/6-31G* program. The results show that the calculated absorption was beyond 440nm, essentially consistent with the experimental value 433 nm.

Keywords fulleropyrrolidine, nanosecond transient spectra, charge-separated state

1 Introduction

Recently, fullerenes connected with functional groups have become important materials for designing new photoelectric devices [1–3]. Fullerenes are characterized by remarkably strong electron-accepting properties and small reorganization energies due to their symmetric structures and special π-electron systems [4]. As electron-acceptors, they can connect the organic donors-dimethylamine [5–7], porphyrins [8], phthalocyanine [9], ruthenium complexes [10], ferrocenes [11, 12], tetrathiafulvalenes [13, 14] and oligothiophenes [15, 16]. The fullerene-based donor-acceptor dyads can create the photoinduced charge-separated states and play an important role in the storage and conversion of solar energy. The efficiency and rates of the electron transfer processes and the lifetime of the charge-separated states are related to the energy of the charge-separated (CS) state, the type of linkage, distance and orientation between the electron-donor and C_{60} moiety [17]. Ito et al. [18, 19] have reported that the fullerene derivatives connected with electron donors played an important role in assisting the electron-transfer ability and hole delocalization. Here, *N*-methyl-2-(*N*-ethylcarbozole)-fulleropyrrolidine (C_{60}–Cz) and *N*-methyl-2-(4'-*N*,*N*-diphenylaminophenyl)-fulleropyrrolidine (C_{60}–TPA) were synthesized under microwave irradiation, in which C_{60} and the amine donors are covalently bonded with short linkage. Photoinduced intramolecular electron transfer processes between fullerene and carbazole have been studied by nanosecond laser flash photolysis. The charge-separated state $C_{60}^{\bullet-}$–$Cz^{\bullet+}$ was observed in the near-IR region with a lifetime of 0.28 μs. The rates and efficiencies of the CS processes were measured by time-resolved fluorescence measurements with changing solvent polarity. The origin of the long lifetimes of the CS state has been revealed by the Marcus parameters experimentally evaluated from the temperature dependence of the CR rate constants [20–22].

2 Materials and methods

2.1 Reagent and instruments

C_{60} (>99.9%) was purchased from 3D Carbon Cluster Material Co. of Wuhan University of China, sarcosine, N-ethylcarbazole-3-carboxaldehyde and 4-(N,N- diphenylamino)benzaldehyde were purchased from Tokyo Casei Inc. Toluene was dried over sodium with dibenzophenone as the indicator, and all other reagents were commercial material. All the cycloaddition reactions were performed under nitrogen. A modified domestic microwave oven perforated

Translated from *Acta Chimica Sinica*, 2005,63(17)(in Chinese)

Wang Tingting(✉) , Zeng Heping(✉)
School of Chemical Science, South China Univers1ty of Technology, Guangzhou 510641, China,
Email: magicglacier@yahoo.com.cn
hezeng@scut.edu.cn

at the top to accommodate a reflux condenser with a 10 cm pipe to avoid microwave leakage was used. ^{1}H NMR spectra were determined in $CDCl_3/CS_2$ with a Varian INOVA 500 MHz spectrometer. Steady-state absorption and fluorescence spectra were measured with a Shimadzu UV-2501 spectrophotometer and a Hitatch FL-2500 spectrofluorophotometer, respectively, at room temperature. IR spectra were recorded on a Perkin Elmer Fourier transform infrared spectrometer as KBr pellets. ESI-MS data were obtained with an LCQ DECA XP mass spectrometer. Cyclic voltammetry measurements were carried out on a BAS-100B potentiostat ultilizing Ag/AgCl as reference electrode, Pt wire as an auxiliary electrode, and a conventional glassy carbon electrode as a working electrode, directly immersed in the PhCN containing 0.1 mol/L TBAP, at a scan rate of 100 mV/s.

Time-resolved fluorescence spectra were measured by a single-photon counting method using a second harmonic generation (SHG, 410 nm) of a Ti:sapphire laser [Spectra–Physics Lasers, Tsunami 3950-L2S, 1.5 ps full width at half-maximum (fwhm)] and a streak scope (Hamamatsu Photonics, C4334-01) equipped with a polychromator (Acton Reasearch, SpectraPro 150) as an excitation source and a detector, respectively.

Nanosecond transient absorption measurements were carried out adopting SHG (532 nm) of Nd: YAG laser (Spectra–Physics Lasers, Quanta-Ray GCR-130, fwhm 6 ns) as an excitation source. For transient absorption spectra in the near-IR region (600 nm～1,600 nm), monitoring light from a pulsed Xe lamp was detected with a Ge-avalanche photodiode (Hamamatsu Photonics, B2834). Photoinduced events in micro- and millisecond time regions were estimated by a continuous Xe lamp (150 W) and an InGaAs-PIN photodiode (Hamamatsu Photonics, G5125-10) as a probe light and a detector, respectively. All the samples in a quartz cell (1×1 cm) were deaerated by bubbling argon through the solution for 15 min.

2.2 Synthesis of *N*-Methyl-2-(*N*-ethylcarbozole)- fulleropyrrolidine(C_{60}–Cz)

The following were dissolved in 100 mL of dry toluene under nitrogen atmosphere: 216 mg of C_{60} (0.3 mmol), 53.4 mg of sarcosine (0.6 mmol) and 268 mg of *N*-ethyl carbazole-3-carboxaldehyde (1.2 mmol). After microwave irradiation for 2 h at 750 W, the brown solution was vaporated to dryness and the raw solid product was purified by flash column chromatography on silica gel (100–200 mesh) to give a dark brown mono-cycloadduct (54.2 mg, 34.98%, based on C_{60} unreacted). R*f*=0.33 (toluene/petroleum ether=2:3). The product can be dissolved in CS_2 and toluene..

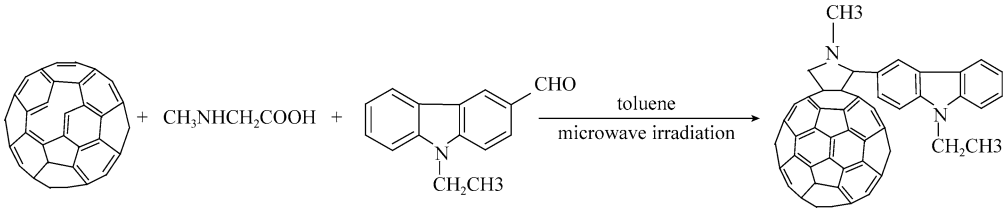

^{1}H NMR (CS2/CDCl3) δ: 7.435～7.017 (m, 7H, ArH), 5.095 (s, 1H), 5.023 (d, *J*=9.75 Hz, 1H), 4.346 (q, *J*=7Hz, 2H), 4.308 (d, *J*=9.75 Hz, 1H), 2.841 (s, 3H, NCH3),1.460 (t, *J*=7 Hz, 3H); FT-IR (KBr) ν: 2,921.59, 2,850.59, 2,769.23, 1,629.37, 1,461.00, 1,382.74, 1,330.61, 1,262.03, 1,231.85, 1,121.14, 801.15, 743.53, 525.92 cm^{-1}; ESI-MS *m*/z: 971 ($M+H^+$).

2.3 Synthesis of N-methyl-2-(4'-N,N-diphenylaminophenyl)-fulleropyrrolidine(C_{60}–TPA)

N-methyl-2-(4'-*N*,*N*-diphenylaminophenyl)-fulleropyrrolidine(C_{60}-TPA) The following were dissolved in 100 mL of dry toluene under nitrogen atmosphere: 216 mg of C_{60} (0.3 mmol), 53.4 mg of sarcosine (0.6 mmol) and 328 mg of 4-(*N*,*N*-dimethylamino)benzaldehyde (1.2 mmol). After microwave irradiation for 2 h at 750 W, the brown solution was vapourated to dryness and the raw solid product was purified by flash column chromatography on silica gel (100–200 mesh) to give a black mono-cycloadduct (29.8 mg, 9.74 %). R*f*=0.51 (toluene/petroleum ether=2:3). The product can be dissolved in CS_2, toluene and tetrahydrofuran.

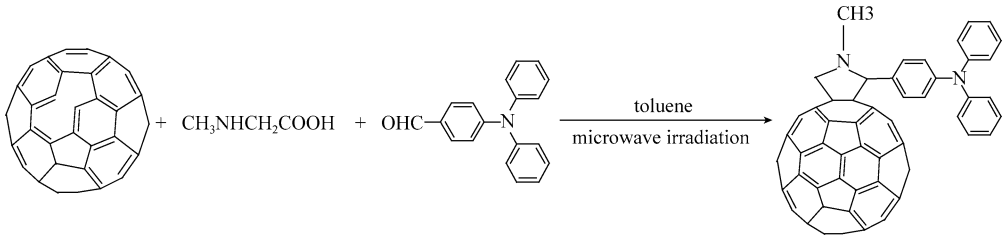

^{1}H NMR (CDCl3/CS2) δ: 7.27–6.95 (m, 14H, ArH), 4.98 [d, *J*=9 Hz, 1H, CH2-(*endo*)], 4.92 (s, 1H, CH), 4.29[d, *J*=9 Hz, 1H, CH2-(*exo*)], 2.88 (s, 3H, NCH3); FT-IR (KBr) ν: 2,921.92, 2,846.15, 2,357.14, 1,623.43, 1,459.74, 1,382.74, 1,273.00, 1,119.38, 614.60, 526.81 cm^{-1}; ESI-MS *m*/z: 1,021 ($M+H^+$).

3 Results and discussion

3.1 Molecular orbital calculation

The geometric parameters of the fulleropyrrolidines were obtained by using the density functional B3LYP/6-31G* method. The optimized structures are shown in Fig. 1. The center-to-center distance (*R*cc) between the C_{60} moiety and the carbazole moiety were estimated to be 0.9 nm. Moreover, Fig. 1 also shows the distribution of the HOMO and LUMO for C_{60}–Cz. The LUMO was mainly located on the C_{60} moiety, while the HOMO was mainly located on the carbazole moiety.

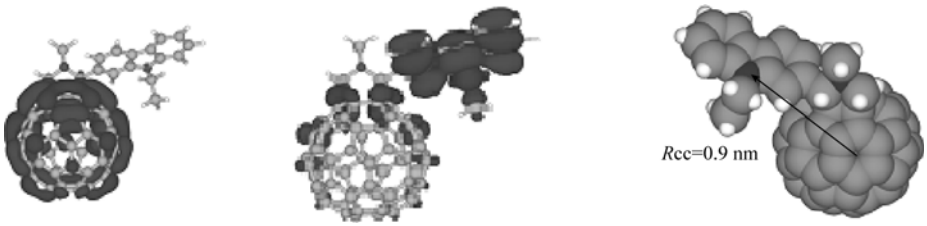

Fig. 1 Optimized structures and electron distributions of LUMO and HOMO of C_{60}—Cz calculated at B3LYP/3-21G* level

3.2 Electrochemical study

The electrochemical properties of C_{60}–Cz and reference compounds (Fig. 2) have been studied by differential-pulse voltammetry (DPV) measurements in benzonitrile (PhCN) as shown in Fig. 3. We can see that the reduction (E_{red}) and oxidation potentials (E_{ox}) were evaluated at -0.84, and +0.68 V vs. Fc/Fc^+ in PhCN. The first negative potentials are attributed to the E_{red} values of the C_{60} moiety and positive potential was assigned to the E_{ox} value of the carbazole moiety by comparing the E_{red} and E_{ox} values of reference compounds. The electrochemical studies confirmed that there is no appreciable electronic interaction between the C_{60} and the carbazole moiety in the ground state.

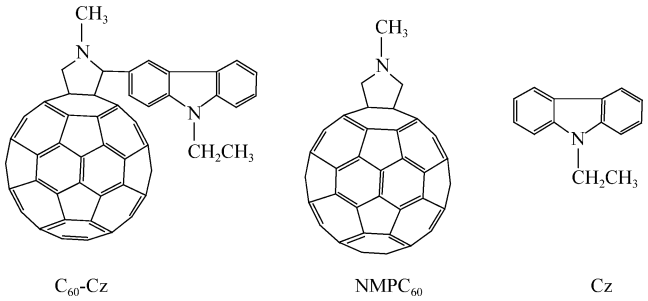

Fig. 2 Molecular structures of the title compound C_{60}–Cz and reference compounds

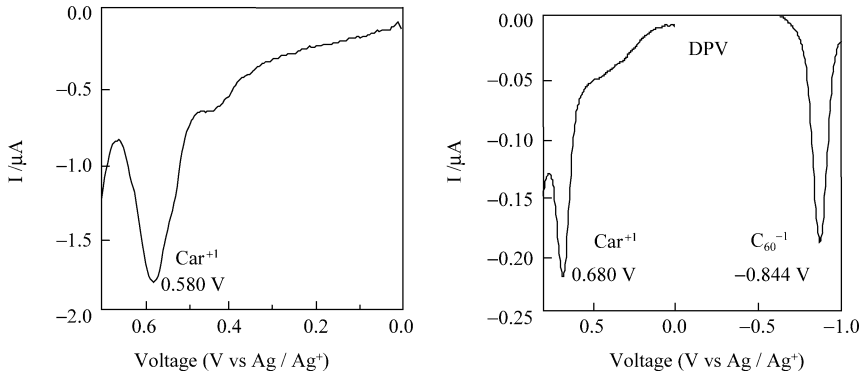

Fig. 3 DPV of cabazole and C_{60}–Cz at 100 mV/s in PhCN at room temperature

3.3 Steady-state absorption spectra

The Steady-state UV/Vis spectra of C_{60}–Cz and reference compounds were measured at 350 nm～800 nm in toluene at room temperature as shown in Fig. 4. The absorption bands of the C_{60} moiety appeared at 705 nm, 435 nm, and shorter than 400 nm, while the absorption of carbazole appeared shorter than 350 nm. The absorption spectra were reasonable superposition of the spectra of the component chromophores making up the molecules and no additional absorption band was observed compared with that of $NMPC_{60}$ and carbazole. This suggests that there is no significant electronic interaction between the individual chromophores in their ground-state configuration. Similar results were obtained in PhCN and DMF. In the fluorescence and transient absorption measurements in our study, the selective excitation was possible with light longer than 400 nm.

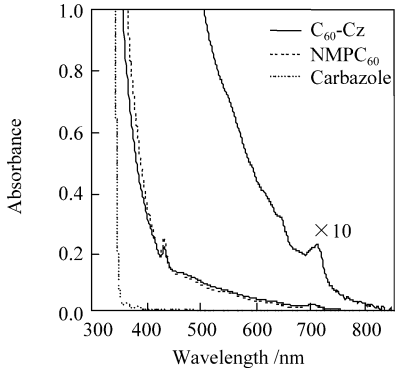

Fig. 4 Steady-state absorption spectra of C_{60}–Cz, reference $NMPC_{60}$, and carbazole (0.1 mol/L) in toluene.

3.4 Steady fluorescence spectra and time-resolved fluorescence spectra

The steady-state fluorescence spectra of C_{60}–Cz was measured in toluene and DMF with the excitation at 520 nm at room temperature as shown in Fig. 5. The C_{60} moiety in C_{60}-EtCz was excited to generate the fluorescence peak at 715 nm. By comparing the fluorescence peak and the absorption peak (705 nm), $^1C_{60}$*–Cz shows a small Stokes shift and the lowest singlet excited energy was 1.75 eV. The fluorescence intensity of $^1C_{60}$*–Cz in toluene was almost the same as that of $NMPC_{60}$, while with the increase of the polarity of the solvent, the fluorescence intensities of $^1C_{60}$*–Cz decreased; i.e., compared with that in toluene, the peak intensity decreased with broadening of the fluorescence band. These observations suggest that CS process predominantly takes place from the excited singlet state $^1C_{60}$*–Cz by excitation with 520 nm light, generating charge-separated state $C_{60}^{\bullet-}$–$Cz^{\bullet+}$.

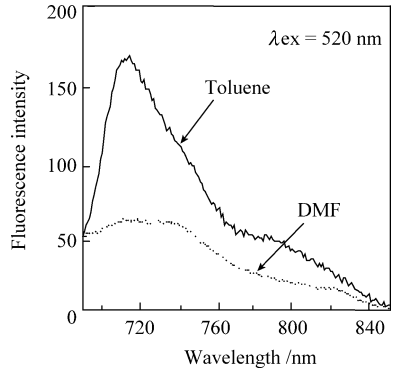

Fig. 5 Steady-state fluorescence spectra of C_{60}–Cz (0.1 mol/L) in toluene and DMF.

The fluorescence lifetimes (τ_f) of C_{60}–Cz and $NMPC_{60}$ were measured using a time-correlated single-photon-counting apparatus with excitation at 410 nm. The fluorescence time profiles of $^1C_{60}$*–Cz in toluene, PhCN and DMF at 700–800 nm are shown in Fig. 6. In toluene the fluorescence decay obeys a single exponential function, giving the τ_f values of 1,400 ps, which is nearly equal to that of $NMPC_{60}$ (1,300 ps). This suggests that only intersystem crossing takes place without charge separation [23]. In PhCN and DMF, fluorescence time profiles show two component exponential decays, giving the two τ_f values. In PhCN, the fast-decaying component had a lifetime, τ_f, of 715 ps (79%), while the lifetime τ_f of the slow decaying component was 1.39 ns (21%). In DMF, similar decay was observed; τ_f of 480 ps (73%) and 1.60 ns (27%) for fast- and slow-decaying, respectively.

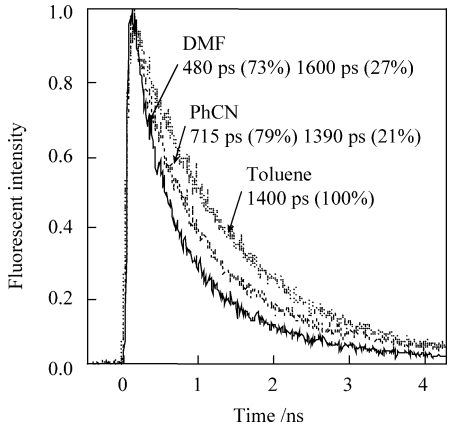

Fig. 6 Fluorescence decay profiles around 700–800 nm of C_{60}–Cz in toluene, PhCN and DMF after 410 nm laser irradiation.

From the E_{ox} and E_{red} values and the Coulomb energy (ΔG_S), the energy levels (ΔG^0_{RIP}) of the radical ion-pair ($C_{60}^{\bullet-}$–$Cz^{\bullet+}$) which are equal to the free-energy changes of charge-recombination (ΔG^0_{CR}) can be calculated by the Weller equations. Thus, the free energy changes for charge-separation (ΔG^0_{CS}) can be calculated by considering the energy levels of the lowest excited state of the C_{60} moiety, when the C_{60} moiety is selectively excited [24].

$$\Delta G^0_{RIP} = -\Delta G^0_{CR} = - E_{ox} + E_{red} - \Delta G_S \quad (1)$$

in which,

$$\Delta G_S = e^2/(4\pi\varepsilon_0))[(1/(2R_+) + 1/(2R_-) - 1/R_{cc})/ \varepsilon_s - (1/(2R_+) + 1/(2R_-))/\varepsilon_R], -\Delta G^0_{CS} = \Delta E_{0\text{-}0} - \Delta G^0_{RIP}$$
$$-\Delta G^0_{CS} = \Delta E_{0\text{-}0} - \Delta G^0_{RIP} \quad (2)$$

In Eqs. 1 and 2, $\Delta E_{0\text{-}0}$ refers to the lowest excited state of the C_{60} (1.75 eV). R_+ and R_- and R_{cc} are radii of cation and anion, and center-to-center distance between donor and acceptor, respectively. The ε_0, ε_s and ε_R refer to vacuum permittivity, dielectric constants of solvents used for rate measurements and the redox potentials measurements, respectively.

The rate constant (k_{CS}) and the quantum yield (Φ_{CS}) for the CS process via $^1C_{60}$*–Cz were calculated using Eqs. 3 and 4, where the $(\tau_f)_{sample}$ and $(\tau_f)_{ref}$ refer to the fluorescence lifetimes of sample and reference, respectively.

$$k_{CS} = (1/\tau_f)_{sample} - (1/\tau_f)_{ref} \quad (3)$$

$$\Phi_{CS} = [(1/\tau_f)_{sample} - (1/\tau_f)_{ref}]/ (1/\tau_f)_{sample} \quad (4)$$

ΔG^0_{CS}, ΔG^0_{CR} values, charge-separation rate-constant (k^S_{CS}) and quantum yield for charge separation (Φ^S_{CS}) are listed in Tables 1 and 2.

Table 1 Fluorescence lifetime (τ_f at 700–800 nm), charge-separation rate-constant (k_{CS}), quantum yield for charge separation (Φ^S_{CS}) via $^1C_{60}$*, and free energy change of charge-separation and charge-reorganization (ΔG^0_{CS}, ΔG^0_{CR})

Solvent	τ_f / ps	k_{CS} / s^{-1}	Φ^S_{CS}	$-\Delta G^0_{CS}$/eV	$-\Delta G^0_{CR}$/eV
Toluene	1,400 (100%)	——	0.00	-0.23	1.98
PhCN	715 (79%)	6.9×10^8	0.49	0.29	1.47
DMF	480 (73%)	1.4×10^9	0.66	0.50	1.25

3.5 Time-resolved nanosecond absorption spectra

Figure 7 shows the transient absorption spectra of C_{60}–Cz in the Vis/NIR region obtained by nanosecond laser light excitation at 532 nm in deaerated PhCN. The peak at 700 nm was attributed to the $^3C_{60}$* moiety in C_{60}–Cz. In the transient spectrum of C_{60}–Cz in DMF (Fig. 8), the transient absorption band around 1,000 nm was attributed to the $C_{60}^{\bullet-}$ moiety [25–27]. The broad absorption bands in the visible region around 620 and 720 nm were assigned to that of the $Cz^{\bullet+}$ moiety in C_{60}–Cz as shown in Fig. 8. Thus, the generation of the CS state ($C_{60}^{\bullet-}$–$Cz^{\bullet+}$) via $^1C_{60}$*–Cz can be confirmed. In PhCN, the absorption band of the $^3C_{60}$* moiety was predominantly observed; however, the absorption intensity of the $^3C_{60}$* moiety was about 1/2, suggesting the competitive process with the intersystem crossing, probably, quick rise and quick decay of the CS state in PhCN.

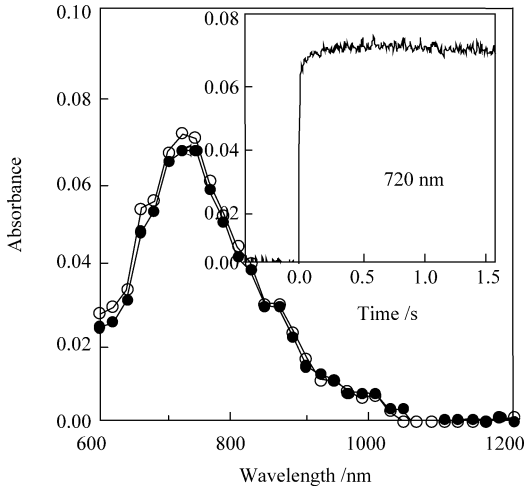

Fig. 7 Nanosecond transient absorption spectra of C_{60}–Cz (0.07 mol/L) observed by 532 nm laser irradiation at 0.1 μs (●) and 1.0 μs (○) in PhCN. Inset: Absorption-time profiles at 720 nm in PhCN.

The time profiles at 1,000 nm in Fig. 8 show that the decay of $C_{60}^{\bullet-}$–$Cz^{\bullet+}$ in the time region till 100 ns obeyed the first-order kinetics with the rate constant of 3.56×10^6 s^{-1} at room temperature. This decay process is attributed to the CR process (k_{CR}) of $C_{60}^{\bullet-}$–$Cz^{\bullet+}$ in DMF; thus from the inverse of the k_{CR} values, the lifetime (τ_{RIP}) of the radical ion-pair ($C_{60}^{\bullet-}$–$Cz^{\bullet+}$) was evaluated to be 280 ns in DMF at room temperature. Compared with the reported τ_{RIP} values for the covalently connected C_{60}-biphenyl amine dyad (220 ns) [7], the τ_{RIP} value of the radical ion-pair ($C_{60}^{\bullet-}$–$Cz^{\bullet+}$) in DMF is longer.

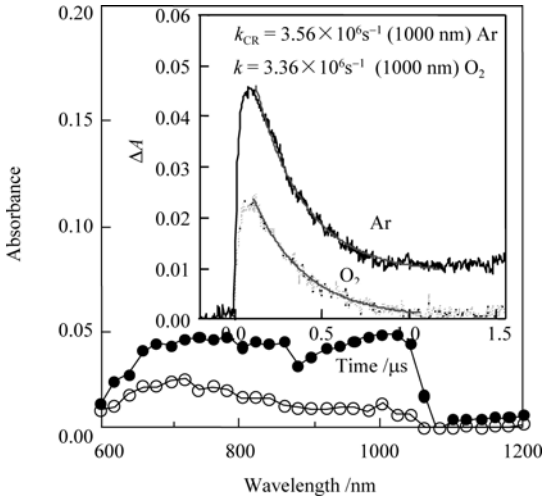

Fig. 8 Nanosecond transient absorption spectra of C_{60}–Cz (0.05 mM) observed by 532 nm laser irradiation in at 0.1 μs (●) and 1.0 μs (○) in DMF. Inset: Absorption-time profiles at 1,000nm in DMF.

The τ_{RIP} value of the C_{60}- (fluorene-diphenylamine) dyad was about 150 ns in DMF at room temperature [18]. In the case of C_{60}-bridge-dimethylaniline systems, τ_{RIP} value was in the range of 8–250 ns, which depended on the kinds and lengths of the bridge molecules [5, 6]. Compared with the fullerene derivatives in which C_{60} and amine dyads are connected with different bridges, $C_{60}^{\bullet-}$–$Cz^{\bullet+}$ with the shot bridge in DMF showed a long τ_{RIP} value.

3.6 Energy diagram of electron transfer process

According to the energy levels of the lowest excited states and the ΔG^0_{CR} and ΔG^0_{CS} values in Table 1, the energy diagram for C_{60}–Cz was illustrated. In Fig. 9, the $E_{0\text{-}0}$ values of the $^1C_{60}$* and $^3C_{60}$* moieties were 1.75 eV and 1.50 eV respectively. With the change of the solvent polarity, the energy levels of $C_{60}^{\bullet-}$–$Cz^{\bullet+}$ were different. From the diagram, it can be seen that the CS state of C_{60}–Cz in toluene is higher than the $^1C_{60}$* and no CS process via $^1C_{60}$* takes place, resulting in the observation of the absorption of $^3C_{60}$* with long lifetime than 20 μs [28]. However, in the polar solvents the energy levels of the charge-separated state decreased, and the CS process via $^1C_{60}$* is possible. In DMF, the CS process via $^3C_{60}$* is also possible, which may be related to the long lifetime of $C_{60}^{\bullet-}$–$Cz^{\bullet+}$, because $C_{60}^{\bullet-}$–$Cz^{\bullet+}$ gains the triplet spin character, when the

precursor is $^3C_{60}$*–Cz [18, 29].

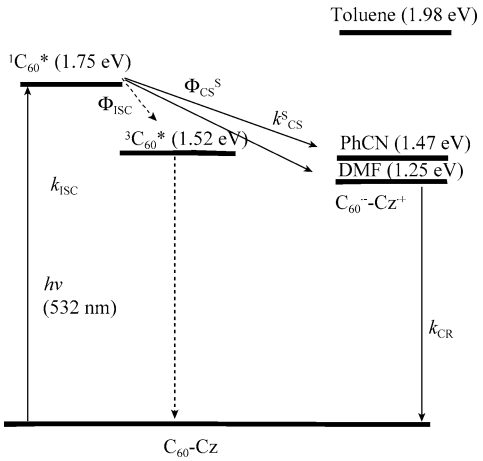

Fig. 9 Schematic energy diagrams and flows of excitation energy and electron of C_{60}–Cz; C_{60} moieties are abbreviated as C_{60} in diagrams.

4 Theoretical study

4.1 Models and methods

We chose C_{60} molecule with Ih-symmetry as the initial input and the center as the location to build the molecular model. The calculations described here were carried out using the Gaussian suite of programs. Molecular geometry of C_{60}-TPA was optimized using the Kohn-Sham density functional theory (DFT) with 6-31G(d) basis sets and Becke three-parameter hybridexchange-correlation functional known as B3LYP. On the basis of the equilibrium geometry of C_{60}-TPA optimized by B3LYP/6-31G(d) method, we employed the ZINDO method to obtain the electronic spectrum.

4.2 Geometry structure

After optimized by the AM1 semiempirical method, the molecular geometry was optimized using the Kohn-Sham density functional theory (DFT) further. The structures and atomic numbering of them were shown in Fig. 10. The calculations showed that sixty carbon atoms occupy 60 vertices of a truncated icosahedron with R_{6-6}=0.1398 and R_{5-6}=0.1451 nm, while the changes of bond lengths of C_{60} moiety, from beginning of additive reaction to the end, are great for the C56 and C57-containing six- or five-membered ring. Bond C56–C57 was changed from double to single, and the bond length varied from 0.1398 nm to 0.1611 nm. The bond lengths of C55–C56, C56–C61, C57–C62 were 0.1534 nm, 0.1556 nm and 0.1587 nm respectively. The properties of the bonds were almost unchanged and the bond lengths were decrescent except bond C56–C57. The results showed that the symmetry of C_{60} was destroyed due to the introduction of the substituent. The bond length of the single bond formed by the two carbon atoms that connected with the substituent is longer than the conjugated bonds. So the two carbon atoms deviated from the plane and the C_{60} sphere became irregular. The dihedral angle of N63–C62–C57–C56 in pyrrolidine rings is 28.144°, and hence the nitrogen atom is at the back of the plane C61–C62–C63. The calculated bond lengths of C–N bond in pyrrolidines are 0.1457 (C61–N63), 0.1462 (C62–N63) and 0.1453 (N64–C63) nm respectively, which are a little longer than that of standard C–N bond.

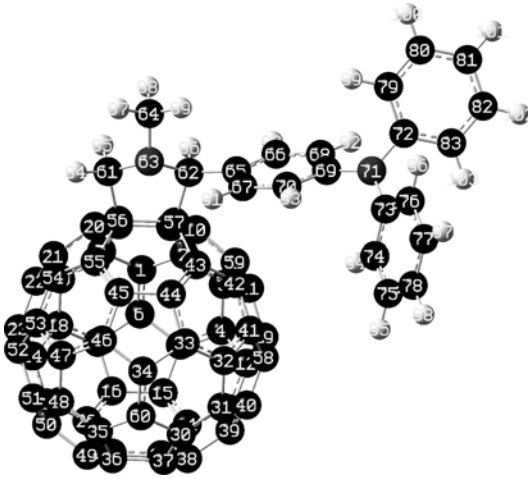

Fig. 10 The optimized structure of compound C_{60}–TPA.

4.3 Electron structure and frontier orbits

In pristine C_{60}, all the carbon atoms are equivalent with net zero charge and the molecule of C_{60} is neutral. But the introduction of pyrrolidine and functional group made the charges on the C_{60} cage redistributed. The net charge values of C_{60} moiety and the pyrrolidine were negative, -0.0893 and -0.0020, respectively, while the net charge of TPA was positive, 0.0913. On the whole, electrons transfer from the donor (TPA) to the acceptor (C_{60} and pyrrolidine).

The electron density distribution in the frontier orbitals heavily determines the properties of the molecules. The frontier orbitals of C_{60}-TPA are shown in Fig. 9. The LUMO is the orbital that could act as the electron acceptor, while the HOMO is the orbital that could act as the electron donor. From the figure, it can be seen that HOMO is mainly located on the TPA, and the LUMO is mainly located on the C_{60} moiety. The results show that the energy data of HOMO and LUMO in C_{60}–TPA were -5.0612 eV and -3.0476 eV, while those in C_{60} were -5.9901 eV and -3.2208 eV, respectively. The LOMO–HUMO energy gap (namely $\Delta E_{LUMO-HOMO}$) of C_{60}–TPA (2.0134 eV) was lower than that of C_{60} (2.7693 eV). This indicated that the electrons were easy to transfer from the occupied orbitals of donors to the virtual orbital of the acceptors, i.e., to excited states.

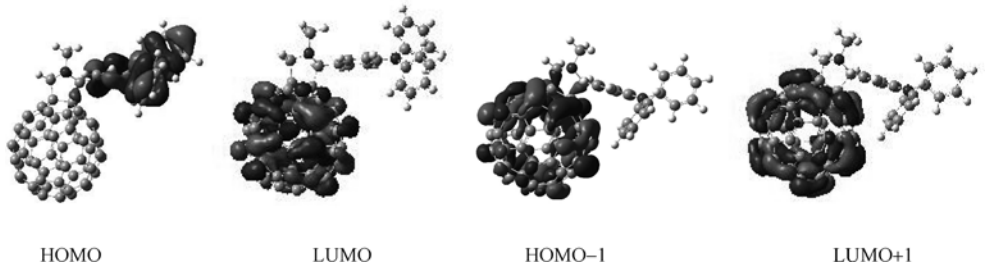

Fig. 11 The frontier molecular orbitals of the compound C_{60}-TPA.

4.4 Electron spectrum

On the basis of the geometry, via the ZINDO method, the electronic spectrum of C_{60}–TPA was calculated. In the ZINDO method, an active space of 14 occupied and 14 virtual orbitals with 197 single-electron excitation configuration and the ground state was included. The main transition, oscillator intensity, corresponding transition wavelength and the transition properties were listed in Table 2 (only the wavelength above 400nm and the oscillator strength above 0.001 were listed).

Table 2 Electronic spectrum data of C_{60}-TPA

λ (cal.)/nm	f	Transition nature	Coefficient	Transition energies/eV	λ (exp.)/nm
579.5	0.0060	177→178	0.661967	2.1397	
485.0	0.0045	176→180	0.494605	2.5566	482.0 nm
		174→180	0.375937		483.0 nm
440.1	0.0016	176→180	0.357117	2.8175	433.1 nm
		173→179	-0.348858		
437.3	0.0033	175→181	0.372051	2.8355	
426.8	0.0134	173→180	-0.574815	2.9053	

The electronic spectrum of C_{60}–TPA (Fig. 12) demonstrates that the main absorption peaks are in the ultraviolet band and retain the characteristic absorption peaks of C_{60}. As shown in Fig. 13, the electronic spectrum of C_{60}–TPA exhibited a new absorption band at a wavelength longer than 400 nm. For C_{60}, the absorption areas are always below 400 nm. Consequently, the weak absorption peak above 400 nm can be taken as a characteristic absorption peak of the fulleropyrrolidine. The gained strong peak 440.1 nm was in good agreement with observed value 433.1 nm. With the introduction of pyrrolidine and the side groups, the symmetry of the systems was decreased and the HOMO–LUMO gap was decreased, and thus the bands were red-shifted and the spectral lines split further with the weak intensity. The characteristic absorption at 440.1 nm was due to the orbital transitions 176(HOMO-1)→180(LUMO+2) and 173→179. The absorption at 579.5 nm was corresponding to the excitation from HOMO→LUMO (177→178).

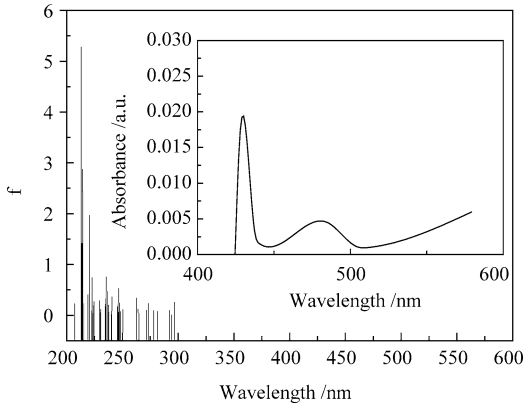

Fig. 12 The electronic spectrum of C_{60}–TPA.

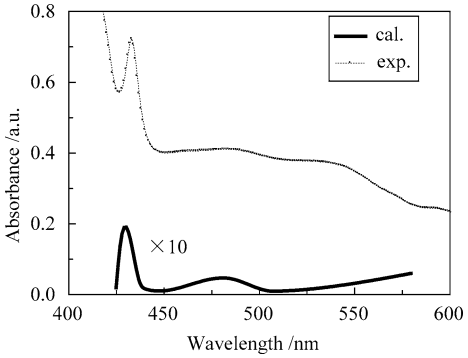

Fig. 13 The electronic spectrum of C_{60}-TPA: calculated data and experimental data (with toluene as the solvent).

5 Conclusion

N-Methyl-2-(*N*-ethylcarbozole)-fulleropyrrolidine was synthesized via the 1,3-dipolar cycloaddition reactions under microwave irradiation. For C_{60} covalently linked to carbazole, photoinduced CS process can predominantly take place via the $^1C_{60}$* moiety, in polar solvents, generating the CS state ($C_{60}^{\bullet-}$–$Cz^{\bullet+}$) in the near-IR region. In DMF, the long lifetime of the charge-separated state was obtained although C_{60} and the amine donor was covalently bonded with short linkage

Acknowledgements The authors acknowledge financial support from the National Natural Science Foundation of China (Nos. 20231020, 20471020). The author also would like to give special thanks to Prof. Osamu Ito and his students of Institute of Multidisplinary Research for Advanced Materials, Tohoku University for his kind help of the measurements.

References

1. Imahori H. and Sakata Y., Donor-linked fullerenes: Photoinduced electron transfer and its potential application, Adv. Mater., 1997, 9(7): 537–546
2. Martín N., Sánchez L., Illescas B. and Pérez I., C_{60}-based electroactive organofullerenes, Chem. Rev., 1998, 98(7): 2527–2548
3. Guldi D. M. and Prato M., Excited state properties of C_{60} fullerene derivatives, Acc. Chem. Res. 2000, 33(10): 695–703
4. Imahori H., Tamaki K., Guldi D. M., Luo C., Fujitsuka M., Ito O., Sakata Y. and Fukuzumi S., Modulating charge separation and charge recombination dynamics in porphyrin-fullerene linked dyads and triads: marcus-normal versus inverted region, J. Am. Chem. Soc., 2001, 123(11): 2607–2617
5. Williams R. M., Zwier J. M. and Verhoeven J. W., Photoinduced intramolecular electron transfer in a bridged C_{60} (acceptor)-aniline (donor) system; Photophysical Properties of the First "Active" Fullerene Diad, J. Am. Chem. Soc., 1995, 117(14): 4093–4099
6. Williams R. M., Koeberg M., Lawson J. M., An Y.-Z., Rubin Y., Paddon-Row M. N. and Verhoeven J. M., Photoinduced electron transfer to C_{60} across extended 3- and 11-bond hydrocarbon bridges: Creation of a long-lived charge-separated state, J. Org. Chem., 1996, 61(15): 5055–5062
7. Komamine S., Fujitsuka M., Ito O., Moriwaki K., Miyata T. and Ohno T., Photoinduced charge separation and recombination in a novel methanofullerene-triarylamine dyad molecule, J. Phys. Chem. A 2000, 104(49): 11497–11504
8. Imahori H., Tamaki K., Araki Y., Sekiguchi Y., Ito O., Sakata Y. and Fukuzumi S., Stepwise charge separation and charge recombination in ferrocene-meso,meso-linked porphyrin dimer-fullerene triad, J. Am. Chem. Soc., 2002, 124(18): 5165–5174
9. Guldi D. M., Ramey J., Martinez-Diaz M. V., de la Escosura A., Torres T., Da Ros T. and Prato M., Reversible zinc phthalocyanine fullerene ensembles, Chem. Commun., 2002, 2(23): 2774–2775
10. Maggini M., Dono A., Scorrano G. and Prato M., Synthesis of [60] fullerene derivative covalently linked to a Ru-thenium(II), J. Chem. Soc. Chem. Commun. 1995, 845–846
11. Zandler M. E., Smith P. M., Fujitsuka M., Ito O. and D'Souza F., Molecular triads composed of ferrocene, C_{60}, and nitroaromatic entities: Electrochemical, computational, and photochemical investigations, J. Org. Chem., 2002, 67(26): 9122–9129
12. Fujitsuka M., Tsuboya N., Hamasaki R., Ito M., Onodera S., Ito O. and Yamamoto Y., Solvent polarity dependence of photoinduced charge separation and recombination processes of ferrocene-C_{60} dyads, J. Phys. Chem. A, 2003, 107(10), 1452–1458
13. Herranz M. A., Ollescas B., Martín N., Luo C. and Guldi D. M., Donor/Acceptor fulleropyrrolidine triads, J. Org. Chem., 2000, 65(18): 5728–5738
14. Kreher D., Hudhomme P., Gorgues A., Luo H., Araki Y. and Ito O., Photoinduced electron transfer processes of a fused C_{60}–TTF–C_{60} dumbbell triad, Phys. Chem. Chem. Phys., 2003, 5(20): 4583.
15. Fujitsuka M., Ito O., Yamashiro T., Aso Y. and Otsubo T., Solvent polarity dependence of photoinduced charge separation in a tetrathiophene-C_{60} dyad studied by pico- and nanosecond laser flash photolysis in the near-IR region, J. Phys. Chem. A, 2000, 104(21): 4876–4881
16. Beckers E. H. A., van Hal P. A., Dhanabalan A., Meskers S. C. J., Knol J., Hummelen J. C. and Janssen R. A. J., Charge transfer kinetics in fullerene-oligomer- fullerene triads containing alkylpyrrole units, J. Phys. Chem. A, 2003, 107(32): 6218–6224
17. Wasielewski M. R., Wiederrecht G. P., Svec W. A. and Niemczyk M. P., Chlorin-based supramolecular assemblies for artificial photosynthesis, Sol. Energy Mater. Sol. Cells 1995, 38:127–134
18. Luo H., Fujitsuka M., Araki Y., Ito O., Padmawar P. and Chiang L. Y., Inter- and intramolecular photoinduced electron-transfer processes between C_{60} and diphenylaminofluorene in solutions, J. Phys. Chem. B, 2003, 107(35): 9312–9318
19. Yamanaka K., Fujitsuka M., Araki Y., Ito O., Aoshima T., Fukushima T. and Miyashi T., Intramolecular photoinduced electron-transfer processes in tetrathienylethylene-quaterthiophene-[60]fullerene triad in solutions, J. Phys. Chem. A, 2004, 108(2): 250–256
20. Marcus R. A., On the theory of oxidation-reduction reactions involving electron transfer. I., J. Chem. Phys., 1956, 24:966-978
21. Marcus R. A., On the theory of electron-transfer reactions. VI. Unified treatment of homogeneous and electrode reactions, J. Chem. Phys. 1965, 43: 679–701
22. Marcus R. A., Sutin N., Electron transfer in chemistry and biology, Biochim. Biophys. Acta 1985, 811: 265–322
23. Sandanayaka S. D. A., Sasabe H., Araki Y., Furusho Y., Ito O. and Takata T., Photoinduced electron-transfer processes between [C_{60}]fullerene and triphenylamine moieties tethered by rotaxane structures. Through-space electron transfer via excited triplet states of [60]fullerene, J. Phys. Chem. A, 2004, 108(24): 5145–5155

24. Weller A., Photoinduced electron-transfer in solution—exciplex and radical ion pair formation free enthalpies and their solvent dependence, Z. Phys. Chem. Neue Folge, 1982, 133, 93–98
25. Arbogast J. W., Foote C. S. and Kao M., Electron transfer to triplet fullerene C_{60}, J. Am. Chem. Soc., 1992, 114(6): 2277–2279
26. Steren C. A., von Willigen H., Biczok L., Gupta N. and Linschitz H., C60 as a photocatalyst of electron-transfer processes: Reactions of triplet C60 with chloranil, perylene, and tritolylamine studied by flash photolysis and FT-EPR, J. Phys. Chem. 1996, 100(21): 8920–8926
27. Luo C., Fujitsuka M., Watanabe A., Ito O., Gan, L., Huang, Y. and Huang, C.-H. J. Chem. Soc., Faraday Trans. 1998, 94, 527
28. Lee M., Song O.-K., Seo J.-C., Kim D., Suh Y. D., Jin S. M. and Kim S. K., Low-lying electronically excited states of C_{60} and C_{70} and measurement of their picosecond transient absorption in solution, Chem. Phys. Lett., 1992, 196: 325–329
29. Yamazaki M., Araki Y., Fujitsuka M. and Ito O., Photoinduced microsecond-charge- separation in retinyl-C_{60} dyad, J. Phys. Chem. A, 2001, 105(38): 8615–8622